Applied Catalysis B: Environmental 224 (2018) 912–918

Contents lists available at ScienceDirect

Applied Catalysis B: Environmental

journal homepage: www.elsevier.com/locate/apcatb

Research Paper

Influence of surface density on the CO_2 photoreduction activity of a DC magnetron sputtered TiO_2 catalyst

F. Fresno[a,**], P. Reñones[a], E. Alfonso[a], C. Guillén[b], J.F. Trigo[b], J. Herrero[b], L. Collado[a], V.A. de la Peña O'Shea[a,*]

[a] Photoactivated Processes Unit, IMDEA Energy Institute, Parque Tecnológico de Móstoles, Avda. Ramón de la Sagra, 3, 28935 Móstoles, Madrid, Spain
[b] Department of Energy, CIEMAT, Avda. Complutense 40, 28040 Madrid, Spain

ARTICLE INFO

Keywords:
CO2 photoreduction
TiO2
DC-magnetron sputtering
Reaction mechanism
Peroxocarbonates

ABSTRACT

Advancing in the photocatalyst scale-up is crucial for the development of highly efficient solar fuels production at industrial scale. Here, we report DC-magnetron sputtering as a suitable technique to produce photocatalytic TiO_2 coatings for CO_2 reduction with a view on process scalability. The crystallinity of the obtained TiO_2 coatings varies with surface density, with amorphous or quasi-amorphous coatings obtained with very low densities, while UV light absorption coefficients show the opposite trend, which has been related to the proportionally higher abundace of surface defects and grain boundaries associated to the small crystal size and/or amorphicity of the lightest coatings. The as-prepared samples lead to the reduction of CO_2 as demonstrated by ^{13}C isotope tracing. An optimum catalyst area density of 1 g/m^2 (by geometric area) is obtained in terms of CO_2 photoreduction production, which is ascribed to a compromise situation between crystallinity and absorption coefficient. Selectivity to the different reaction products also varies with the coating characteristics, with amorphous or quasi-amorphous light coatings favouring methanol formation, in contrast with the preferred CO evolution in heavier, crystalline ones. Raman spectroscopy reveals the formation of peroxo and peroxocarbonate species on the photocatalyst surface as oxidation products during the CO_2 reduction, the accummulation of which is proposed to be related to the observed catalyst deactivation.

1. Introduction

The development of CO_2 valorization strategies has become a crucial goal in order to fulfil the climate pledges that were raised by the Paris Agreement and ratified in Marrakesh in the last Conference of the Parties (COP22). The big challenge lies in the high stability of the CO_2 molecule, which requires a large amount of energy to be activated. Therefore, the key for the promotion of CO_2 transformation technologies is their integration with renewable energy sources. Photocatalytic CO_2 reduction, one of the processes encompassed in the so-called Artificial Photosynthesis, aims at producing sustainable fuels using water as reducing agent, and is mainly based on the use of semiconductor catalysts under mild operation conditions and using sunlight as the driving energy source [1–3]. One of the main bottlenecks for the development of this process resides in the difficulty for establishing comparison criteria for catalytic activities, reaction conditions and irradiation geometries, which redounds to the current lack of optimized parameters with a view on process scalability [4,5]. Therefore, in order to achieve a successful photofuels production it is necessary to tackle the challenge in a holistic manner that identifies and solves the barriers and needs inherent to a large-scale development.

In this sense, it is crucial to advance in the fabrication and scale-up of photocatalytic materials using techniques that provide uniform and pure films with high deposition rates and short processing times. In any case, in order to lead to an efficient scale-up, it would be necessary to use preparation procedures adequate for large areas. In recent years, great advances have been realized in procedures, both chemical and physical, for the large-scale preparation of nanostructured materials, which can be applied to the scale-up of devices for artificial photosynthesis [1–3,6]. In this respect, thin film conformations offer advantages such as an optimal surface conformation and material quantity minimization in comparison with powdered materials. These large-area techniques are especially indicated for CO_2 photoreduction since they do not introduce undesired organic compounds on the catalyst surface. Additionally, the optimization of highly dispersed active sites provided by these methods may lead to an improvement of the photocatalytic

* Corresponding author.
** Co-Corresponding author.
E-mail addresses: fernando.fresno@imdea.org (F. Fresno), victor.delapenya@imdea.org (V.A. de la Peña O'Shea).

https://doi.org/10.1016/j.apcatb.2017.11.022
Received 26 August 2017; Received in revised form 8 November 2017; Accepted 9 November 2017

activity.

However, in the scale-up of a process, especially in the specific case of photo-activated processes, an increase of the layer thickness leads to a threshold value above which little or no dependence is found. This threshold depends on the nature of the light and the depth, structure and optical absorption coefficient (α) of the film, which arises from two main factors: 1) at high depth the light intensity becomes so weak that no significant number of electron-hole pairs can be produced [7,8]; and 2) the proportion of the charge carriers produced at high depth that reach the surface before recombination is low due to their limited diffusion length [7]. Therefore, not all thin-film techniques are appropriate for a fruitful integration in pilot and demonstration plants, and currently those based on, e.g., nanolithography, are only adequate for fundamental studies. However, others like reactive DC magnetron sputtering (DC-MS), starting from conductive substoichiometric oxides or pure metal targets, are powerful methods to synthesize oxides over large areas and at high deposition rates by setting the deposition conditions in the metal-oxide transition region. This would enable these techniques to be transferred from the laboratory to larger scales. The DC-MS technique allows the deposition of well adherent, transparent films with a controllable density at high deposition rate, with good reproducibility and control over the chemical, structural, morphological and textural properties of the final materials [8–11]. From the manufacturing point of view, it is also interesting that the technique allows the use of flexible substrates like carbon fibre and polymer foils, among others. The deposition onto flexible supports facilitates the transport and manipulation in shape-adaptable devices [12,13] and enables a low-cost mass production by roll-to-roll based continuous fabrication processes [14,15]. In addition, it allows the preparation of tailor-made photocatalytic coatings with improved reactivity due to the control of the nanostructure from amorphous to even preferentially facet-oriented [16,17].

The aim of the present study is to assess DC magnetron sputtering as a suitable method to prepare photocatalytic coatings for CO_2 reduction with a view on process scalability and to study the effect of the coating conditions on the structure, optoelectronic properties and photoactivity of the catalyst, in order to propose an optimum situation for the pursued reaction. For that purpose, results obtained using coatings with different area densities are reported and related to the coating characteristics. Regarding the photocatalyst choice, TiO_2 still represents the most appropriate material for photocatalysis [18–20]. In the particular case of CO_2 reduction, TiO_2 is clearly preponderant, being employed in more than 50% of the works published to date [21]. Therefore, it appears as the most suitable option for scalability studies.

2. Experimental

2.1. Synthetic procedures

TiO_2 catalysts were prepared at room temperature by reactive DC magnetron sputtering of a metallic target (Ti, 99.6% purity). The deposition processes were performed simultaneously on glass fibre (GF) wafers with 132.7 cm^2 geometrical area and on soda-lime glass (SLG) substrates with 2 × 2 cm^2 area taken as references for characterization purposes only (Table 1). The sputtering chamber was first evacuated to a base pressure of 3.0×10^{-4} Pa, and then raised three orders of magnitude by introducing the working gas (Ar) and the reactive gas (O_2) through separated mass-flow controllers, according to the proportion that was optimized in a previous work for the attainment of anatase TiO_2 layers [11]. The sputtering power density was maintained at 8 W/cm^2 and the sputtering time was varied to obtain film thicknesses ranging from 0.05 to 1.79 μm, as has been verified by profilometric measurements on the SLG substrates. In this way, the mass deposited on the GF substrates has been increased from 3 to 100 mg (geometrical area densities between 0.23 and 7.54 g/m^2). The superficial to geometrical area ratio increases from 1.01 for SLG to 1.35 for GF, as it has been obtained by profilometry on several bare substrates. This has been used to estimate the equivalent film thickness on GF in relation to the thickness value measured on the respective SLG partner, as it is shown in Table 1.

Table 1
Supported TiO_2 samples prepared by DC-MS. Samples numbered the same were obtained simultaneously.

GF samples	SLG samples	TiO_2 area density (gm^{-2})	TiO_2 film thickness on SLG (μm)	Equivalent film thickness on GF (μm)
GF1	SLG1	0.23	0.05	0.04
GF2	SLG2	0.53	0.12	0.09
GF3	SLG3	1.06	0.25	0.19
GF4	SLG4	2.11	0.50	0.37
GF5	SLG5	3.17	0.75	0.56
GF6	SLG6	4.22	1.00	0.75
GF7	SLG7	7.54	1.79	1.34

2.2. Characterization methods

The obtained samples were characterized by X-ray diffraction (XRD) using Cu K_α radiation in a Panalytical EMPYREAN. Diffraction angles were compared with International Centre for Diffraction Data Powder Diffraction Files (PDF) for phase identification. Mean crystallite sizes were calculated by using the Scherrer formula. The surface topography has been examined with a Park XE-100 atomic force microscope (AFM).

Raman spectra were recorded at room temperature using a JASCO NRS-5000/7000 series spectrometer with an excitation wavelength of 532 nm. For Raman shift and band width determination, the most intense band of the anatase spectrum was fitted to an asymmetric variation of the pseudo-Voigt profile [22]. Total transmittance T and reflectance R of the coatings were measured in the wavelength range between 250 and 1800 nm in a Perkin–Elmer Lambda 9 spectrometer equipped with an integrating sphere. Then, the absorptance A(%) was deduced using A(%) = 100 − T(%) − R(%) and the absorption coefficient α has been calculated as α = (1/t) ln{100/(T(%) + R(%)} [23], taking t as the film thickness on SLG or GF substrates.

2.3. CO_2 photoreduction procedure

Gas-phase photocatalytic experiments were conducted in a continuous-flow mode. The TiO_2-sputtered GF wafers were introduced in a stainless steel reactor with an effective volume of 280 mL and provided with a borosilicate glass window for irradiation. The reaction conditions were set at 2 bar and 50 °C maintaining a CO_2:H_2O molar ratio of 7.25. In-line gas chromatography analyses (GC Agilent 7890A) were performed to quantify the reaction products every 22 min. The photocatalytic measurements were performed using four UV lamps of 6 W each (λ_{max} = 365 nm), with a total irradiance of 27.95 Wm^{-2} under 400 nm (Fig. S1). Before starting the experiments, the reactor was firstly outgassed at 50 °C and then purged with Ar (100 mL/min) for 1 h to remove any residual compounds weakly adsorbed on the catalyst surface. Then, the reactor was flushed with the CO_2–H_2O mixture for 1 h to establish an adsorption-desorption balance at the reaction temperature. Prior to illumination, the reactor was pressurized and kept at the reaction flow rate. All photocatalytic tests were carried out over an irradiation period of 18 h.

Isotope tracer experiments were carried out in a 15.6 mL stainless steel reactor with a borosilicate glass window operated in batch mode. After outgassing, $^{13}CO_2$ (Cambridge Isotope Laboratories, Inc., 99.2% ^{13}C, < 1% ^{18}O) and H_2O were introduced in the reactor at 50 °C with a total pressure of 2 bar. After 30 min irradiation with a 6 W UV lamp (λ_{max} = 365 nm), the gas was extracted to a quadrupole mass spectrometer (Pfeiffer OMNISTAR) for analysis (Fig. S2).

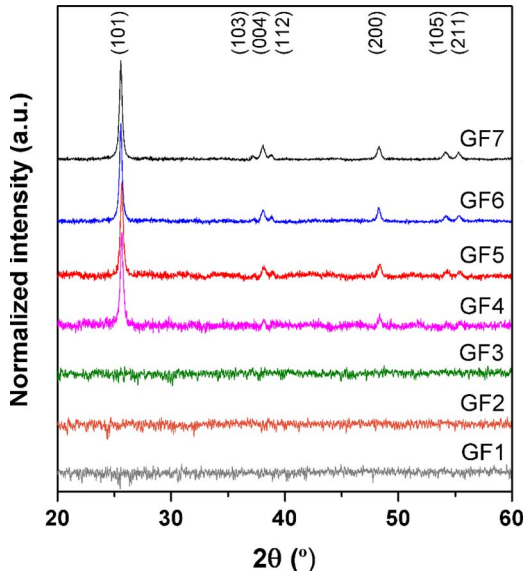

Fig. 1. XRD patterns obtained for the TiO_2 coatings on glass fibre wafers. The peak identification has been made according to the ICDD PDF file 00-021-1272 for anatase.

3. Results and discussion

3.1. Characterization of the photocatalytic coatings

XRD patterns of GF samples (Fig. 1) show clear diffraction peaks for TiO_2 area densities above ca. 2 g/m^2. Below that charge, amorphous titania or crystalline structures with exceedingly small crystal size or mass percentage could be present but not observed by XRD. Otherwise, the characteristic diffraction peaks of the anatase phase are always detected, without any reflections that could be ascribed to other TiO_2 phases, as expected from the used deposition conditions [11]. In SLG samples (Fig. S3), amorphous behaviour is observed for the thinnest films, although the limit for the appearance of diffraction peaks is lower than in GF samples. This suggests that the absence of these peaks in GF samples with lower titania contents is related either to the detection limit of the technique or to small crystalline domains, rather than to an amorphous coating. In order to shed light on this point, Raman spectra were recorded on GF samples. Fig. 2 reveals that peaks corresponding to vibrations of the anatase lattice at ca. 146 (E_g; strong), 195 (E_g; weak), 393 (B_{1g}; medium), 512 (A_{1g} + B_{1g}; medium) and 634 (E_g; medium) [24], are present in all cases except for the sample with the lowest titania charge, which looks amorphous to Raman spectroscopy too [25].

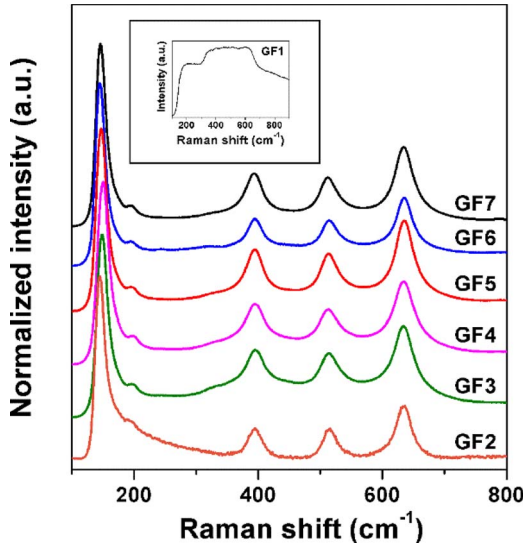

Fig. 2. Raman spectra of the TiO_2 coatings on glass fibre wafers.

Regarding structural aspects, details of the (101) peak measured for the various SLG samples (see Fig. S4A) reveal that the position of the peak changes slowly towards lower diffraction angles as the film thickness increases. By comparing the interplanar spacing, d, for each sample with the standard anatase value (ICDD PDF #00-021-1272), d_0, it can be pointed out that the TiO_2 coatings show compressive structural distortion, $(d - d_0)/d_0 < 0$, which is about 0.7% for t = 0.25 μm and decreases to 0.1% for t = 1.79 μm. A similar observation can be made regarding the GF samples (Fig. S4B), although the 2ϑ displacement is not monotonic. About the structural distortion origins, it should be noted that some tensile strain is expected to act by the grain coalescence mechanism that is common to any thin film regardless of the synthesis technique or the material [26], together with compressive stress linked to the incorporation of high energy atoms or particles that depend on the specific deposition conditions [26,27]. The structural distortion observed experimentally results from the competition between such independent mechanisms, and the compressive strain predominates for the thinnest TiO_2 coatings in the present deposition conditions. Small variations are found in average crystallite sizes for both GF and SLG samples (27 ± 2, 30 ± 1 nm, respectively) without a clear trend against TiO_2 charge. A phonon confinement analysis [28] of the anatase Raman band at ca. 146 cm^{-1} was carried out by representing Raman shifts (ν) and band widths (Γ) against the reciprocal of crystal size (1/S) and fitting the corresponding points to the equations:

$$\nu = \nu_0 + k_1(1/S)^{1.55} \quad (1)$$

$$\Gamma = \Gamma_0 + k_2(1/S)^{1.55} \quad (2)$$

The fittings (Fig. S5) reveal that both vary with crystal size as expected from phonon confinement, indicating that no further defects, apart from those inherent to the nanostructure, are introduced by the present preparation method, in good accordance with XRD observations.

Previous works of TiO_2 deposited over SLG have shown good adhesion properties and the root mean square roughness shows a correlation with the porosity [11]. Here, in the case of the coatings deposited on glass fibre, even when a good distribution of the catalyst is apparent to the naked eye (Fig. 3A: blue-grey colour under UV light is indicative of reduced TiO_2), a detailed SEM characterization (Fig. 3B–C), together with AFM images (Fig. S6), reveal that such distribution is not homogenous, leading to the formation of TiO_2 aggregates. Therefore, due to the porous nature of the support, the film thickness and grain size are less homogeneous on GF with respect to SLG samples. Nevertheless, this porosity facilitates the reagents transport and allows an intimate interaction with the photocatalysts.

Fig. S7A shows the absorptance spectra obtained for the various TiO_2 coatings on the GF substrates. For the thickest TiO_2 samples, the absorptance falls abruptly below 3.5 eV, but it starts to decrease slowly at higher energies when the coating thickness is diminished. The absorption coefficient corresponding to the same samples is represented in Fig. S7B, where it can be seen that higher α values are achieved with the lightest TiO_2 coatings. Such increment in the absorption coefficient is observed in the overall radiation spectra and thus it should be related to additional absorption by surface defects and grain boundaries, which are proportionally more abundant in thinner coatings, as it is illustrated by the AFM images shown in Fig. S6. Taking into account that UV lamps (λ_{max} = 365 nm) have been used for the photoreduction experiments, the absorptance and the absorption coefficient at such wavelength (named A365 nm and α365 nm) have been represented as a function of the TiO_2 area density in Fig. 4. This evidences the fast variation occurring with low TiO_2 charges, and then a slower evolution with the thicker coatings. Then, the highest absorption coefficients correspond

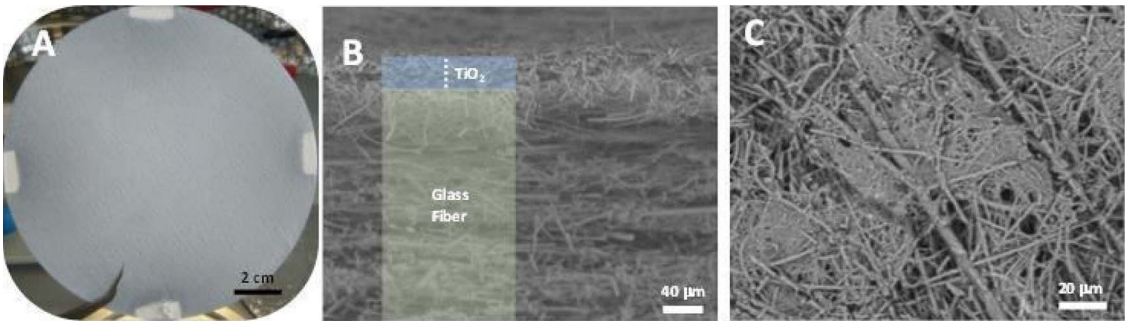

Fig. 3. (A) Sample GF3 after UV irradiation. SEM microphotographs of the (B) lateral and (C) frontal view.

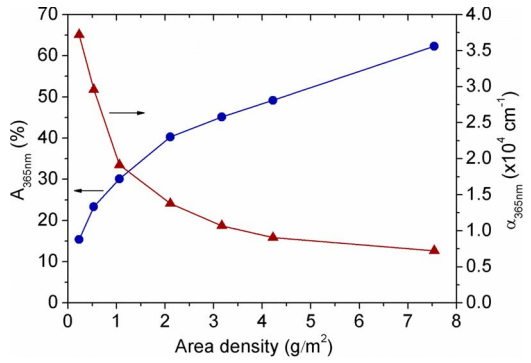

Fig. 4. Evolution of the absorptance and the absorption coefficient obtained at 365 nm radiation wavelength for the TiO_2 coatings deposited with various thicknesses on GF substrates.

to the amorphous coating, in the same way as observed for other sputtered TiO_2 layers [12,29].

3.2. CO_2 photoreduction

The performance of TiO_2-coated GF samples was evaluated in CO_2 photoreduction under UV light using water as electron donor. The main reaction products are CO and CH_3OH plus trace amounts of CH_4, along with H_2 coming from H_2O reduction competing with CO_2 for conduction band electrons. No products were found after performing blank reactions without any catalyst under dark and UV–vis illumination, or in the presence of catalyst in dark conditions, discarding any CO_2 or H_2O conversion due to thermal or photochemical reactions or to thermal catalysis. Previous studies using powdered anatase TiO_2 photocatalysts in the same reaction conditions have also shown high selectivities towards the formation of syngas (CO + H_2) [30,31].

Fig. 5(A–C) shows the kinetic profiles of the main products for all catalysts. The maximum production rates of CO are reached between 3 and 6 h of irradiation depending on the sample. On the other hand, H_2 and CH_3OH show a quasi-stable rate in most of the samples. As a general trend, the evolution of the products is more stable in time with the smaller catalyst charges, while with high area densities the production decreases with time.

The cumulative outcomes of the different reaction products over the whole studied period, obtained by integration of the kinetic curves, are gathered in Table 2. In order to compare overall photocatalytic activities regardless of the product distribution, the value "C-products" is defined as the molar sum of the CO_2 reduction products, and represents the total CO_2 moles converted into products. An initial comparison of C-products with the different samples reveals that the photocatalytic performance of the TiO_2 coating exhibits a high dependence on the catalyst area density even if the activities are referred to the catalyst mass unit. Thus, an optimum value is achieved with the GF3 sample which contains TiO_2 surface density of ca. 1 g/m^2. Below and above this value, lower conversions are observed. In addition, the lower and upper surface density limits, represented by samples GF1 and GF7, give rise to similar CO_2 conversions. Counteracting effects seem therefore to account for the observed order of activities. The structural characterization discussed above revealed that the lower TiO_2 charge limit results in an amorphous or quasi-amorphous coating, and that crystallinity-related features are better resolved as the area density, or the films thickness in SLG samples, increases. On the other hand, Fig. 4C has revealed that the absorption coefficient decreases in the GF1 → GF7 series. The optimal area density value appears thus as a compromise situation between these factors. This optimal catalyst coverage has significant implications in process scale-up [32]. Under the present conditions, the obtained overall apparent quantum yields vary from 0.002 to 0.03%, which is of the same order than previously reported results of CO_2 photoreduction over TiO_2 [33–36], although the values reported in the literature vary not only with the type of catalyst, but also with reactor configuration, reaction conditions and irradiation sources.

The highest selectivity is observed towards CO production except in the case of GF1 catalyst (Fig. 5D). This behaviour in the CO_2 reduction reaction has been previously observed by these authors and is a usual outcome when using oxide photocatalysts without a metallic co-catalyst [30,31,37]. However, the product distribution is highly dependent on the characteristics of the coatings. With high area densities, selectivities to different carbon products are similar to those obtained with powdered TiO_2 catalysts [31], with CO representing more than 90% of the carbon-containing products, a small proportion of methanol and even smaller of methane. However, this situation changes with the lightest TiO_2 coatings, and in the GF1 sample methanol selectivity reaches 16% of all products, which represents nearly 30% of the C-containing ones. As explained above, XRD and Raman studies have depicted that this sample exhibits an amorphous nature or extremely small crystals. In this respect, the existence of low-coordinated Ti cations in amorphous titania has been postulated from theoretical studies as well as from X-ray absorption and electron paramagnetic resonance results [38–40]. In line with this, the cation coordination number (N_c), estimated for the present amorphous and crystalline samples obtained on SLG substrates through the analysis of the reflectance interferences [41–43] (Fig. S8) by the parametrization of the refractive index by means of the dispersion equation given by the Wemple-DiDomenico oscillator model:

$$(n^2 - 1) - 1 = [E_0 - E^2]/E_d E_0, \quad (3)$$

where n is the refractive index (Fig. S8A), E_0 is the single oscillator energy, E_d the dispersion energy, and E the photon energy. The dispersion energy is attained from the linear fits plotted in Fig. S8B, as it contains information about density and coordination number in the films considered as a mixture of amorphous and crystalline phases, through the relation:

$$E_{da}/E_{dx} = (\rho_a/\rho_x)(N_{ca}/N_{cx}), \quad (4)$$

where ρ is the density, and subscripts a and x refer to amorphous and

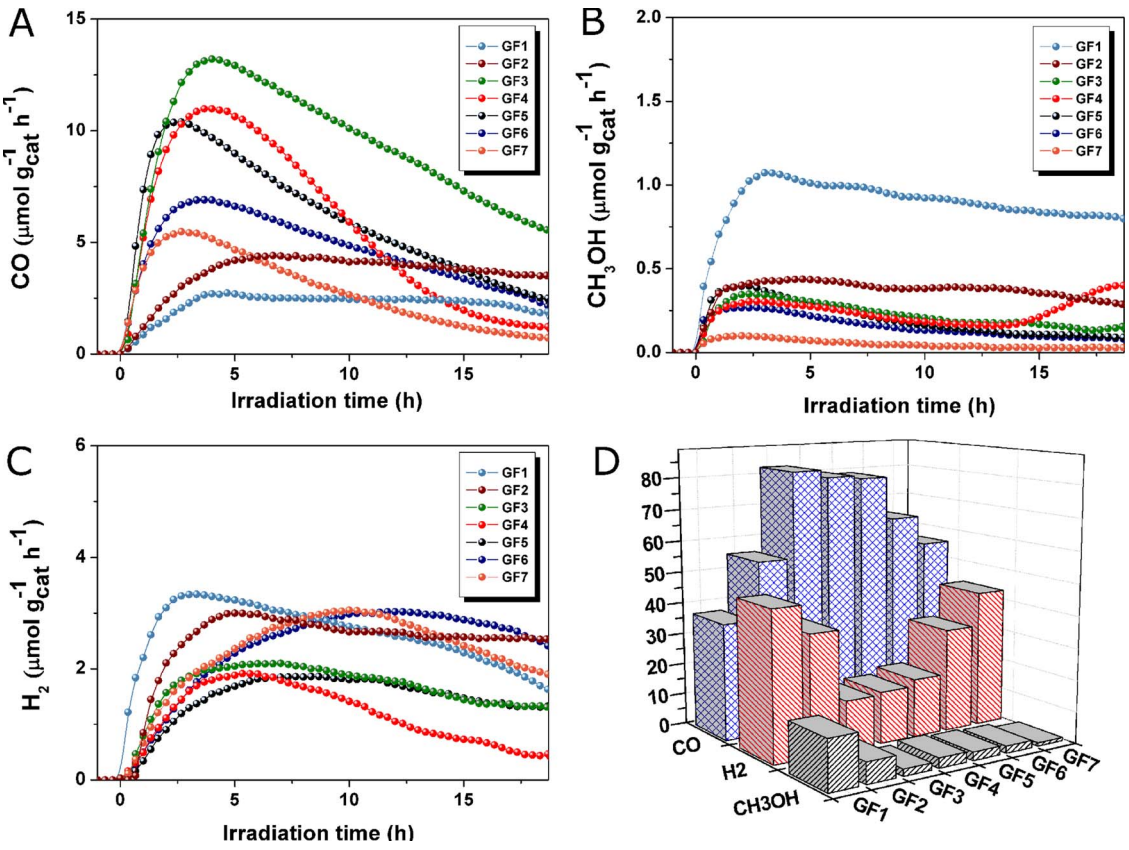

Fig. 5. Temporal evolution of the main reaction products in CO_2 photoreduction over GF samples: A) CO, B) CH_3OH and C)H_2, along 18 h of irradiation. D) Selectivities towards these products.

Table 2
Cumulative production (μmol g_{cat}^{-1}) for all catalysts in the CO_2 + H_2O reaction after 18 h of UV irradiation.

Sample	H_2	CO	CH_3OH	CH_4	C-products
GF1	50.0	39.6	16.8	0.7	57.1
GF2	47.2	68.9	8.3	0.5	77.7
GF3	33.9	180.6	4.7	0.2	185.5
GF4	24.0	117.2	4.6	1.0	122.8
GF5	28.4	121.9	4.1	0.2	126.2
GF6	46.0	91.8	3.2	0.1	95.1
GF7	45.1	58.0	1.0	0.2	59.2

crystalline phases, respectively. For the present samples, the N_{ca} values shown in Fig. S8 B have been calculated from the bulk TiO_2 values N_{cx} = 6.0, E_{dx} = 24.96 eV and the packing density of each film ρ_a/ρ_x = P = $(n_{550} - 1)/1.6$, taken the *n*-value at 550 nm wavelength. In the case of the SLG1 sample, enough maxima were not obtained for calculation. Overestimation of N_c in thick samples is common to the method [41]. Therefore, the thickest coatings have not been included in Fig. S8B. These studies suggest a decrease in Nc for the thinnest cases. It has been argued that isolated TiO_2 particles, with a relatively high proportion of tetrahedrally coordinated Ti centres, favour the formation of methanol in photocatalytic CO_2 reduction reactions, both in powders and in thin films [44,45], which has been related to improved charge transfer and low concentration of surface OH groups. The change in selectivity observed here with the lightest coatings may therefore be related to the amorphicity or small size of the TiO_2 structures improving the charge transfer processes and the production of highly electron-demanding products such as methanol.

Further experiments were performed to assure that the observed production is due to carbon dioxide and does not arise from carbon-containing impurities present in the samples. The presence of these

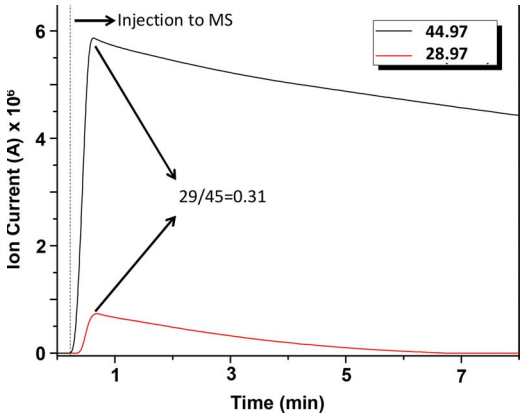

Fig. 6. Selected ion monitoring in the mass spectrometric analysis after photocatalytic reduction of $^{13}CO_2$.

impurities was first ruled out by elemental analysis (Table S1). In line with this, $^{13}CO_2$ photocatalytic reduction followed by mass spectrometric analysis (Fig. 6) shows an increase in the ratio between the ions with mass 29 ($^{13}CO^+$) and 45 ($^{13}CO_2^+$). This ratio is 0.18 when directly measuring the mass spectrum of the $^{13}CO_2$ cylinder, while it increases to 0.31 when $^{13}CO_2$ is introduced in the photoreactor and the reactor content is analyzed after the photocatalytic reduction. This increase is attributed to the formation of ^{13}CO.

Taking into account that Raman spectroscopy is a surface sensitive technique, a series of spectra were acquired to determine the surface changes and adsorbed species before and after reaction (Fig. 7). Raman experiments in fresh samples show that TiO_2 surface is covered by different carbon species adsorbed from its contact with ambient air. The observed bands are assigned to bidentate carbonate b−CO_3^{2-} at 1045,

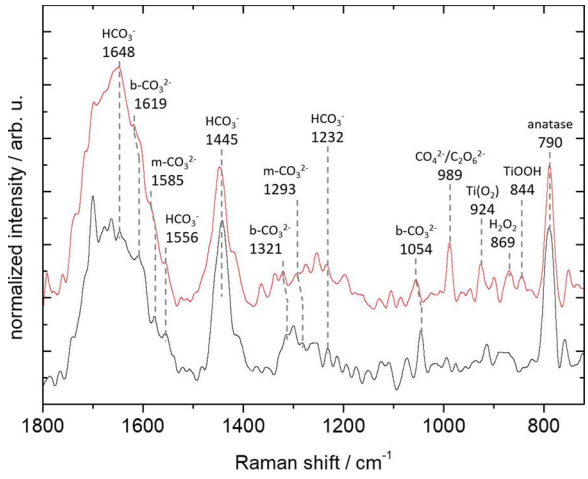

Fig. 7. Raman spectra of TiO_2 anatase before (down) and after (up) reaction.

1313 (ν_s C—O) and 1608 (ν_{as} C—O) cm^{-1} [46,47]; monodentate carbonate m—CO_3^{2-} at 1284 (ν_s C—O) and 1576 (ν_{as} C—O) cm^{-1} [47–49] and bicarbonate HCO_3^- at 1232 (δ OH), 1445 (ν_s CO), 1556 (ν_{as} C—O) and 1648 (ν_{as} C—O) cm^{-1} [46–48].After reaction, some changes are observed on the TiO_2 surface due to an increase of CO_3^{2-} and HCO_3^- species. Furthermore, carbonate bands show a blue shift of c.a. 9 cm^{-1} probably due to structural rearrangements. It is worth highlighting the appearance of a new Raman band at 989 cm^{-1} corresponding to the ν_{O-O} vibrational mode of peroxocarbonate species ($CO_4^{2-}$and $C_2O_6^{2-}$) [50]. In addition, peaks at 924, 869 and 844 cm^{-1} were assigned by Nakamura et al. to the ν_{O-O} vibrational mode of surface peroxo species $Ti(O_2)$, physisorbed H_2O_2 and surface hydroperoxo species TiOOH respectively [51].The formation of peroxo species on TiO_2 as a pathway for the oxygen evolution reaction has been previously reported in photoredox reaction literature [51–54]. In addition, Sayama et al. proposed a speculative mechanism for oxygen evolution in CO_2 photoreduction via peroxocarbonate species [55], which may act as hole scavengers [56,57]. However, to the best of our knowledge, this is the first time that peroxocarbonates are detected by spectroscopic techniques for this reaction on TiO_2. These experiments lead us to conclude that the generation of both peroxo and peroxocarbonate species arising from hole capture by CO_3^{2-} and HCO_3^- species could prevent H_2O from being further oxidized into free O_2. The accumulation of these peroxidized species on TiO_2 surface could also cause its deactivation.

4. Conclusions

DC magnetron sputtering has demonstrated to be a highly applicable technique for the deposition of TiO_2 coatings for CO_2 photocatalytic reduction. Structural and optoelectronic characterization reveals that decreasing catalyst area density leads to crystalline coatings down to a limit below which the deposited material appears to be amorphous, which also influences the light absorption properties of the catalytic system. Performance tests in gas-phase photocatalytic CO_2 reduction reveals an optimum area density of 1 g/m^2 in terms of CO_2 conversion, which is ascribed to compromise situation between crystallinity and absorption coefficient. In turn, selectivities towards the different reaction products is also highly influenced by the TiO_2 loading, with amorphous or quasi-amorphous coatings favouring methanol formation in contrast with the preferred CO evolution in the rest of cases. Therefore, this technique opens up the possibility of not only optimizing catalyst usage towards an industrial implementation in terms of overall CO_2 reduction outcome, but also tuning the selectivity of the process at the expense of conversion. Raman spectroscopy reveals the formation of peroxo and peroxocarbonate species on the surface of the photocatalyst during the CO_2 reduction reaction, which could prevent H_2O, CO_3^{2-} and HCO_3^- from being further oxidized into free O_2. The accumulation of these species on TiO_2 surface could also cause its deactivation.

Acknowledgements

This work, developed under the HyMAP project, has received funding from the European Research Council (ERC) under the European Union's Horizon 2020 research and innovation programme (grant agreement No. 648319). The results reflect only the authors' view and the Agency is not responsible for any use that may be made of the information they contained. Further support has been received from the Spanish Ministry of Economy and Competitiveness trough the *SolarFuel* (ENE2014-55071-JIN) and Ra-PHUEL (ENE2016-79608-C2-1-R) projects. F.F. thanks financial support from the Amarout-II PEOPLE-COFUND Marie Skłodowska-Curie Action. Support from the Repsol Technology Centre is gratefully acknowledged.

Appendix A. Supplementary data

Supplementary data associated with this article can be found, in the online version, at http://dx.doi.org/10.1016/j.apcatb.2017.11.022.

References

[1] V.A. de la Peña O'Shea, D.P. Serrano, J.M. Coronado, From Molecules to Materials – Pathways to Artificial Photosynthesis, in: E. Rozhkova, K. Ariga (Eds.), Springer, London, 2015.
[2] Peng, G. Reid, H. Wang, P. Hu, Perspective: Photocatalytic reduction of CO_2 to solar fuels over semiconductors, J. Chem. Phys. 147 (2017) 030901.
[3] X. Chang, T. Wang, J. Gong, CO_2 photo-reduction: Insights into CO_2 activation and reaction on surfaces of photocatalysts, Energy Environ. Sci. 9 (2016) 2177–2196.
[4] R.K. de Richter, T. Ming, S. Caillol, Fighting global warming by photocatalytic reduction of CO_2 using giant photocatalytic reactors, Renew. Sustain. Energy Rev. 19 (2013) 82–106.
[5] M. Motegh, J.R. van Ommen, P.W. Appel, M.T. Kreutzer, Scale-up study of a multiphase photocatalytic reactor –degradation of cyanide in water over TiO_2, Environ. Sci. Technol. 48 (2014) 1574–1581.
[6] P. Reñones, A. Moya, F. Fresno, L. Collado, J.J. Vilatela, V.A. de la Peña O'Shea, Hierarchical TiO_2 nanofibres as photocatalyst for CO_2 reduction: Influence of morphology and phase composition on catalytic activity, J. CO_2 Util. 15 (2016) 24–31.
[7] H. Tada, M. Tanaka, Dependence of TiO_2 photocatalytic activity upon its film thickness, Langmuir 13 (1997) 360–364.
[8] K. Eufinger, D. Poelman, H. Poelman, R. De Gryse, G.B. Marin, Photocatalytic activity of DC magnetron sputter deposited amorphous TiO_2 thin films, Appl. Surf. Sci. 254 (2007) 148–152.
[9] H. Poelman, D. Poelman, D. Depla, H. Tomaszewski, L. Fiermans, R. De Gryse, Optical properties of MgO–TiO_2 amorphous composite films, Surf. Sci. 940 (2001) 482–485.
[10] K. Eufinger, E.N. Janssen, H. Poelman, D. Poelman, R. De Gryse, G.B. Marin, The effect of argon pressure on the structural and photocatalytic characteristics of TiO_2 thin films deposited by D.C. magnetron sputtering, Thin Solid Films 515 (2006) 425–429.
[11] C. Guillén, J. Montero, J. Herrero, Anatase and rutile TiO_2 thin films prepared by reactive DC sputtering at high deposition rates on glass and flexible polyimide substrates, J. Mater. Sci. 49 (2014) 5035–5042.
[12] P. Peerakiatkhajohn, W. Onreabroy, C. Chawengkijwanich, S. Chiarakorn, Preparation of visible-light-responsive TiO_2 doped Ag thin film on PET plastic for BTEX treatment, J. Sustain. Energy Environ. 2 (2011) 121–125.
[13] H.C. Weerasinghe, F. Huang, Y.B. Cheng, Fabrication of flexible dye sensitized solar cells on plastic substrates, Nano Energy 2 (2013) 174–189.
[14] G. Hashmi, K. Miettunen, T. Peltola, J. Halme, I. Asghar, K. Aitola, M. Toivola, P. Lund, Review of materials and manufacturing options for large area flexible dye solar cells, Renew. Sustain. Energy Rev. 15 (2011) 3717–3732.
[15] G. Suchaneck, O. Volkonskiy, G. Gerlach, Z. Hubicka, A. Dejneka, L. Jastrabik, S. Günther, E. Schultheiss, Deposition of PZT on copper-coated polymer films, Ceram. Mater. 62 (2010) 456–460.
[16] S. Davíðsdóttir, J. Petit, M. Mermoux, R. Shabadi, S. Canulescu, K.P. Almtoft, K. Dirscherl, R. Ambat, Interfacial structure and photocatalytic activity of magnetron sputtered TiO_2 on conducting metal substrate, ACS Appl. Mater. Interfaces 6 (2014) 22224–22234.
[17] B.I. Stefanov, G.A. Niklasson, C.G. Granqvist, L. Österlund, Quantitative relation between photocatalytic activity and degree of (001) orientation for anatase TiO_2 thin films, J. Mater. Chem. A. 3 (2015) 17369–17375.
[18] M.D. Hernández-Alonso, F. Fresno, S. Suárez, J.M. Coronado, Development of alternative photocatalysts to TiO_2: challenges and opportunities, Energy Environ. Sci. 2 (2009) 1231–1257.

[19] W. Tu, Y. Zhou, Z. Zou, Photocatalytic conversion of CO_2 into renewable hydrocarbon fuels: state-of-the-art accomplishment, challenges, and prospects, Adv. Mater. 16 (2014) 4607–4626.
[20] D. Chen, X. Zhang, A.F. Lee, Synthetic strategies to nanostructured photocatalysts for CO_2 reduction to solar fuels and chemicals, J. Mater. Chem. A. 3 (2015) 14487–14516.
[21] [dataset], http://www.artleafs.eu, (2017).
[22] A.L. Stanick, E.B. Brauns, A simple asymmetric lineshape for fitting infrared absorption spectra, Vib. Spectrosc. 47 (2008) 66–69.
[23] K. Bindu, P.K. Nair, Semiconducting tin selenide thin films prepared by heating Se–Sn layers, Semicond. Sci. Technol. 19 (2004) 1348–1353.
[24] T. Zeng, Y. Qiu, L. Chen, X. Song, Microstructure and phase evolution of TiO_2 precursors prepared by peptization-hydrolysis method using polycarboxylic acid as peptizing agent, Mater. Chem. Phys. 56 (1998) 163–170.
[25] N.R. Mathews, E.R. Morales, M.A. Cortés-Jacome, J.A. Toledo Antonio, TiO_2 thin films–Influence of annealing temperature on structural, optical and photocatalytic properties, Sol. Energy 83 (2009) 1499–1508.
[26] G.C.A.M. Janssen, Stress and strain in polycrystalline thin films, Thin Solid Films 515 (2007) 6654–6664.
[27] A.J. Detor, A.M. Hodge, E. Chason, Y. Wang, H. Xu, M. Conyers, A. Nikroo, A. Hamza, Stress and microstructure evolution in thick sputtered film, Acta Mater. 57 (2009) 2055–2065.
[28] S. Kelly, F.H. Pollak, M. Tomkiewizc, Raman spectroscopy as a morphological probe for TiO_2, J. Phys. Chem. B. 101 (1997) 2730–2734.
[29] C.H. Wei, C.M. Chang, Polycrystalline TiO_2 thin films with different thicknesses deposited on unheated substrates using RF magnetron sputtering, Mater. Transact. 52 (2011) 554–559.
[30] L. Collado, P. Jana, B. Sierra, J.M. Coronado, P. Pizarro, D.P. Serrano, Enhancement of hydrocarbon production via artificial photosynthesis due to synergetic effect of Ag supported on TiO_2 and ZnO semiconductors, Chem. Eng. J. 224 (2013) 128–135.
[31] L. Collado, A. Reynal, J.M. Coronado, D.P. Serrano, J.R. Durrant, V.A. de la Peña O'Shea, Effect of Au surface plasmon nanoparticles on the selective CO_2 photoreduction to CH_4, Appl. Catal. B: Environ. 178 (2014) 177–185.
[32] R.J. Braham, A.T. Harris, Review of major design and scale-up considerations for solar photocatalytic reactors, Ind. Eng. Chem. Res. 48 (2009) 8890–8905.
[33] Z. Xiong, Z. Lei, S. Ma, X. Chen, B. Gong, Y. Zhao, J. Zhang, C. Zheng, J.C.S. Wu, Photocatalytic CO_2 reduction over V and W codoped TiO_2 catalyst in an internal-illuminated honeycomb photoreactor under simulated sunlight irradiation, Appl. Catal. B: Environ. 219 (2017) 412–424.
[34] L. Liu, Y. Jiang, H. Zhao, J. Chen, J. Cheng, K. Yang, Y. Li, Engineering coexposed {001} and {101} facets in oxygen-deficient TiO_2 nanocrystals for enhanced CO_2 photoreduction under visible light, ACS Catal. 6 (2016) 1097–1108.
[35] Z. Xiong, H. Wang, N. Xu, H. Li, B. Fang, Y. Zhao, J. Zhang, C. Zheng, Photocatalytic reduction of CO_2 on Pt^{2+}-Pt^{*}/TiO_2 nanoparticles under UV/Vis light irradiation: a combination of Pt^{2+} doping and Pt nanoparticles deposition, Int. J. Hydrog. Energy 40 (2015) 10049–10062.
[36] P. Liou, S. Chen, J.C.S. Wu, D. Liu, S. Mackintosh, M. Maroto-Valer, R. Linforth, Photocatalytic CO_2 reduction using an internally illuminated monolith photoreactor, Energy Environ. Sci. 4 (2011) 1487–1494.
[37] S. Xie, Q. Zhang, G. Liu, Y. Wang, Photocatalytic and photoelectrocatalytic reduction of CO_2 using heterogeneous catalysts with controlled nanostructures, Chem. Commun. 52 (2016) 35–59.
[38] H. Zhang, B. Chen, J.F. Banfield, Atomic structure of nanometer-sized amorphous TiO_2, Phys. Rev. B. 78 (2008) 214106.
[39] H. Yoshitake, T. Sugihara, T. Tatsumi, XAFS study on the local structure of Ti in amorphous mesoporous titania, Phys. Chem. Chem. Phys. 5 (2003) 767–772.
[40] J.M. Coronado, A.J. Maira, J.C. Conesa, K.L. Yeung, V. Augugliaro, J. Soria, EPR study of the surface characteristics of nanostructured TiO_2 under UV irradiation, Langmuir 17 (2001) 5368–5374.
[41] C. Guillén, J. Montero, J. Herrero, Influence of N-doping and air annealing on the structural and optical properties of TiO_2 thin films deposited by reactive DC sputtering at room temperature, J. Alloy. Compd. 647 (2015) 498–506.
[42] S.H. Wemple, M. DiDomenico, Behavior of the electronic dielectric constant in covalent and ionic materials, Phys. Rev. B. 3 (1971) 1338–1351.
[43] S.H. Wemple, Refractive-Index behavior of amorphous semiconductors and glasses, Phys. Rev. B. 7 (1973) 3767–3777.
[44] H. Yamashita, Y. Fujii, Y. Ichihashi, S.G. Zhang, K. Ikeue, D.R. Park, K. Koyano, T. Tatsumi, M. Anpo, Selective formation of CH3OH in the photocatalytic reduction of CO_2 with H_2O on titanium oxides highly dispersed within zeolites and mesoporous molecular sieves, Catal. Today. 45 (1998) 221–227.
[45] Y. Shioy, K. Ikeue, M. Ogawa, M. Anpo, Synthesis of transparent Ti-containing mesoporous silica thin film materials and their unique photocatalytic activity for the reduction of CO_2 with H_2O, Appl. Catal. A: Gen. 254 (2003) 251–259.
[46] W. Su, J. Zhang, Z. Feng, T. Chen, P. Ying, C. Li, Surface phases of TiO_2 nanoparticles studied by UV raman spectroscopy and FT-IR spectroscopy, J. Phys. Chem. C 112 (2008) 7710–7716.
[47] G. Martra, Lewis acid and base sites at the surface of microcrystalline TiO_2 anatase: relationships between surface morphology and chemical behaviour, Appl. Catal. A Gen. 200 (2000) 275–285.
[48] G. Busca, V. Lorenzelli, Infrared spectroscopic identification of species arising from reactive adsorption of carbon oxides on metal oxide surfaces, Mater. Chem. 7 (1982) 89–126.
[49] H. Zhao, L.J. Liu, Y. Andino Li, Bicrystalline TiO_2 with controllable anatase?brookite phase content for enhanced CO_2 photoreduction to fuels, J. Mater. Chem. 1 (2001) 8209–8216 (A).
[50] L.J. Chen, C.J. Lin, J. Zuo, L.C. Song, C.M. Huang, First spectroscopic observation of peroxocarbonate/peroxodicarbonate in molten carbonate, J. Phys. Chem. B 108 (2004) 7553–7556.
[51] R. Nakamura, Y. Nakato, Primary intermediates of oxygen photoevolution reaction on TiO_2 (Rutile) particles: revealed by in situ FTIR absorption and photoluminescence measurements, J. Am. Chem. Soc 126 (2004) 1290–1298.
[52] E. Karamian, S. Sharifnia, On the general mechanism of photocatalytic reduction of CO_2, J. CO_2 Util. 16 (2016) 194–203.
[53] A. Fujishima, X. Zhang, D.A. Tryk, TiO_2 photocatalysis and related surface phenomena, Surf. Sci. Rep. 63 (2008) 515–582.
[54] R. Nakamura, A. Imanishi, K. Murakoshi, Y. Nakato, In situ FTIR studies of primary intermediates of photocatalytic reactions on nanocrystalline TiO_2 films in contact with aqueous solutions, J. Am. Chem. Soc. 125 (2003) 7443–7450.
[55] K. Sayama, H. Arakawa, Effect of carbonate salt addition on the photocatalytic decomposition of liquid water over Pt–TiO_2 catalyst, J. Chem. Soc. Faraday Trans. 93 (1997) 1647–1654.
[56] N.M. Dimitrijevic, B.K. Vijayan, O.G. Poluektov, T. Rajh, K.A. Gray, H. He, P. Zapol, Role of water and carbonates in photocatalytic transformation of CO_2 to CH_4 on titania, J. Am. Chem. Soc. 133 (2011) 3964–3971.
[57] A. Pougin, M. Dilla, J. Strunk, Identification and exclusion of intermediates of photocatalytic CO_2 reduction on TiO_2 under conditions of highest purity, Phys. Chem. Chem. Phys. 18 (2016) 10809–10817.